CHEMBIOCHEM

DOI: 10.1002/cbic.200800070

# Layer-By-Layer Assembly of Viral Nanoparticles and Polyelectrolytes: The Film Architecture is Different for Spheres Versus Rods

Nicole F. Steinmetz,*[a, e] Kim C. Findlay,[b] Timothy R. Noel,[c] Roger Parker,[c] George P. Lomonossoff,[d] and David J. Evans[d]

*The development of tuneable thin film assemblies that contain (bio)nanoparticles is an emerging field in nanobiosciences/nanotechnology. Our research focuses on the utilisation of viral nanoparticles (VNPs) as tools and building blocks for materials science. In previous reports we studied multilayered arrays of chemically modified cowpea mosaic virus (CPMV) particles and linker molecules. To extend these studies and to gain more insights into the architecture of the arrays, we report here on the construction of multilayered assemblies of native plant viral particles and polyelectrolytes. We specifically addressed the question of whether the shape of the VNPs influences the overall structures of the arrays. To study this, we have chosen two particles with similar surface properties but different shapes: CPMV was used as a sphere-like VNP, and tobacco mosaic virus (TMV) served as a rod-shaped VNP. The multilayers were self-assembled on solid supports through electrostatic interactions. Multilayer build-up was followed by quartz crystal microbalance with dissipation monitoring and UV/Vis spectroscopy. Scanning electron microscopy was used to characterize the topologies of the thin films. Our studies show that shape indeed matters. Incorporation of CPMV in alternating arrays of VNPs and polyelectrolytes is demonstrated; in stark contrast, TMV particles were found to be excluded from the arrays, and floated atop the architecture in an ordered structure.*

## Introduction

A major objective in nanosciences/nanotechnology is the construction of ordered systems, such as spatially organized arrays. The electrostatic layer-by-layer (LbL) technique has been found to be a versatile tool for the design of highly tuneable and ultrathin films made up of alternately deposited cationic and anionic polyelectrolytes.[1] Furthermore, it has been demonstrated that functional molecules can be incorporated into these ultrathin films. These include functional proteins,[2] nucleic acids,[3] metallic and semiconducting nanoparticles,[4] redox-active moieties[5] and virus particles.[6–8] This approach thus has great potential for the design of functional devices with applications in fields such as sensors, optoelectronics, drug delivery, coatings for biomedical applications and other coatings. Viral nanoparticles (VNPs) in particular have appealing features to be exploited for use in materials science. VNPs are in general very robust, monodisperse nanoparticles that can be modified either by genetic manipulation or by chemical bioconjugation techniques. Viral capsids consist of multiple copies of identical protein subunits, and thus offer multiple and various sites for attachment and display of functional molecules.[9]

Although VNPs have been extensively studied, only a few studies have focussed on the immobilization and incorporation of VNPs in thin film assemblies. We have recently demonstrated that multilayered VNP arrays can be constructed with the well characterized icosahedral plant virus cowpea mosaic virus (CPMV). CPMV particles covalently modified with biotin and fluorescent dyes were self-assembled into an alternating array of CPMV and streptavidin by using an LbL approach; the biotin moieties served as linker and allowed construction through streptavidin interaction, and different fluorescent labels enabled sequential detection.[10] In a subsequent study we analysed the assembly mechanism and the mechanical properties of such arrays in more detail. It was found that inter- and intramolecular cross-linking, and hence the densities of the CPMV arrays, can be tightly tuned by carefully adjusting linker length and density.[11]

Douglas and Young studied VNP multilayer assembly with the plant virus cowpea chlorotic mottle virus (CCMV).[8] Alternating arrays of biotinylated CCMV particles and streptavidin were constructed. Deposition of CCMV particles and polyelec-

[a] *Dr. N. F. Steinmetz*
*Department of Biological Chemistry, John Innes Centre*
*Colney, Norwich, NR4 7UH (UK)*

[b] *K. C. Findlay*
*Department of Cell and Developmental Biology*
*John Innes Centre, Colney, Norwich, NR4 7UH (UK)*

[c] *T. R. Noel, Dr. R. Parker*
*Institute of Food Research, Norwich Research Park*
*Colney, Norwich, NR4 7UA (UK)*

[d] *Dr. G. P. Lomonossoff, Dr. D. J. Evans*
*Department of Biological Chemistry, John Innes Centre*
*Colney, Norwich, NR4 7UH (UK)*

[e] *Dr. N. F. Steinmetz*
*Present address: Department of Cell Biology*
*The Scripps Research Institute, 10550 North Torrey Pines Road*
*La Jolla, CA 92037 (USA)*
*Fax: (+1) 858-784-7979*
*E-mail: nicoles@scripps.edu*

  

trolytes (here poly-L-lysine) by LbL assembly was also achieved; this led to the formation of an alternating thin film with stable incorporation of the spherical VNPs.[8] LbL studies with the carnation mottle virus (CarMV) and polyelectrolytes (here poly(allylamine) and poly(styrene sulfonate)) were in good agreement. The construction of an alternating multilayered thin film with stable incorporation of the spherical CarMV particles has also been reported.[7]

Findings with rod-shaped VNPs contrasted with the results obtained with spherical VNPs (CCMV and CarMV). The assembly of the rod-shaped bacteriophage M13 and polyelectrolytes (here poly(ethyleneimine) and poly(acrylic acid)) resulted in an architecture in which the M13 particles were found to be floating on top of the film; even after deposition of further polyions on top of the bound VNPs the particles were not stably incorporated into the films, but were instead found to be excluded from the structure and assembled in an ordered fashion on top of the film.[6]

Here, we have investigated whether the particle shape (sphere versus rod) influences binding to polyelectrolyte substrates and the subsequent incorporation. To address this, we compared the LbL assembly of sphere-like and rod-shaped VNPs into polyelectrolyte multilayers. We chose the cationic poly(ethyleneimine) (PEI, linear, $M_W$ 25 kDa) and the anionic poly(acrylic acid) (PAA, $M_W$ 90 kDa) as polyions to build up the multilayers. CPMV served as the sphere-like VNP, and tobacco mosaic virus (TMV) particles—also a plant virus—were chosen as rod-shaped VNPs. CPMV particles have diameters of approximately 30 nm, while TMV particles are rod-shaped with diameters of 18 nm and lengths of 300 nm. Besides their differences in shape, the two particles have similar surface properties, such as surface charge: the isoelectric point (pI) of CPMV particles is between pH 3.4 and 4.5,[12] TMV particles have a pI of ~3.5.[12] The multilayer build-up was followed by quartz crystal microbalance with dissipation monitoring (QCMD) and UV/Vis spectroscopy. The surface topology was studied by scanning electron microscopy (SEM).

## Results and Discussion

### Comparison of CPMV and TMV adsorption on initial films of polyelectrolytes by QCMD

Firstly, the adsorption behaviour of CPMV and TMV particles onto thin films of polyelectrolytes was studied. The pIs of CPMV and TMV particles are comparable and lie at pH 3.4–4.5 and pH ~3.5, respectively.[12] Experiments were performed at pH 5.0; at this pH both particle types have a net negative charge. In addition, at pH 5.0 50% of the amines of PEI are protonated;[13] this allows binding of negatively charged objects through electrostatic interactions. The VNPs were deposited onto 2.5 bilayers of $(PEI\text{-}PAA)_2$-PEI (note: it is assumed that after deposition of 2.5 bilayers of polyelectrolytes, 2.5 bilayers were indeed formed). The initial film was chosen to be 2.5 bilayers (rather than a single PEI layer), in order to make sure that full surface coverage was achieved. The terminating layer was the polycation PEI; this allowed binding of the negatively charged VNPs through electrostatic interactions.

Multilayer build-up and deposition of the VNPs was monitored by QCMD. We have recently shown that QCMD is a feasible technique for characterization of VNP multilayer assemblies.[11] QCMD monitors changes in resonance frequency ($\Delta f$) and changes in dissipation ($\Delta D$) in situ and in real time. Changes in $\Delta f$ correlate with changes in mass ($\Delta m$); a decrease in $\Delta f$ equates to an increase in $\Delta m$. Changes in $\Delta D$ give information about the viscoelastic properties of the array: the more viscoelastic the structure, the higher the energy losses and hence $\Delta D$. Theoretical models have been developed; the QCMD response to rigid films and viscoelastic (Voigt) films have been modelled by the approaches of Sauerbrey[14] and Voinova et al.,[15] respectively. A small mass ($\Delta m$) deposited on the sensing surface of the quartz crystal will cause a decrease in $\Delta f$, which is proportional to $\Delta m$ if the mass: 1) is small in relation to the mass of the crystal, 2) is evenly distributed, 3) does not slip on the surface and 4) is sufficiently rigid and/or thin to have negligible internal friction. In this case the Sauerbrey equation applies:[14]

$$\Delta m = -C\ \Delta f/n \qquad (1)$$

in which $C$ is the sensitivity constant ($C = 17.7\ ng\,cm^{-2}\,Hz^{-1}$ for a 5 MHz crystal), and $n$ is the overtone with $n = 1, 3, 5$, etc.

If the energy losses ($\Delta D$) are high, the data can be analysed by being fitted to the viscoelastic Voigt model; in this more complex model the thickness, density and elastic shear modulus of the adsorbed layers are taken into account.[15]

Figure 1 shows the changes in $\Delta f$ and $\Delta D$ monitored as a function of time for CPMV and TMV deposition. The continuous decrease in $\Delta f$ equates to an increase in $\Delta m$ and therefore indicates that polyelectrolyte multilayers were self-assembled on the solid support and that VNPs were adsorbed on top of the ultrathin films. On the basis of the Sauerbrey equation,[14] $\Delta m$ deposited for each VNP at each pH was calculated. Theoretical values for the coverage ($\Gamma$) for CPMV and TMV were estimated on the basis of the size and molecular weight of the particles; calculations were based on the formation of a closely packed monolayer. The expected theoretical coverages of CPMV and TMV are 1.33 $\mu g\,cm^{-2}$ and 1.30 $\mu g\,cm^{-2}$, respectively. Experimentally ascertained values were higher: the $\Delta m$ values found were 2.45 $\mu g\,cm^{-2}$ for CPMV and 3.37 $\mu g\,cm^{-2}$ for TMV. The apparent higher mass uptake for both VNPs might indicate the formation of multi- rather than monolayers. However, when working with biomolecules one has to consider hydrodynamically coupled water and water molecules that are entrapped in cavities of the assembly,[16] which could also explain the apparent higher mass uptake. For both CPMV and TMV stable irreversible binding was observed; the desorption rates after being washed with buffer or water were negligible.

The binding modes of CPMV and TMV are different. Adsorption of sphere-like CPMV particles is accomplished within less than 2 min. In stark contrast, it takes about 30 min to reach a stable plateau (maximum binding) when the rod-shaped TMV particles are deposited (Figure 1). These striking differences in

  

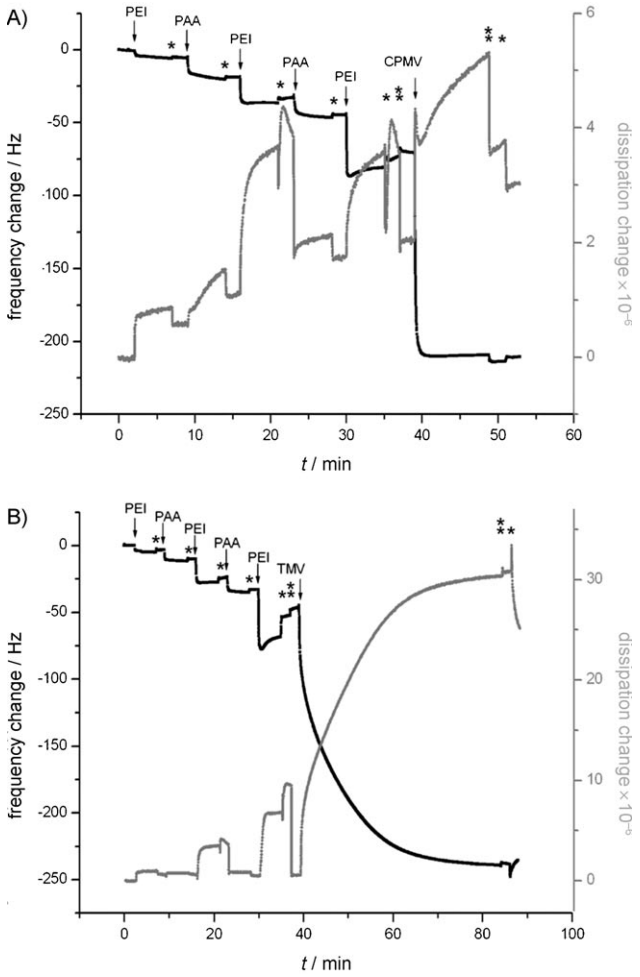


**Figure 1.** Quartz crystal microbalance frequency and dissipation shift during the build-up of polyelectrolyte multilayers and viral nanoparticles (VNPs); 2.5 bilayers of the polyelectrolytes linear poly(ethyleneimine) (PEI) and poly(acrylic acid) (PAA) were built up as base film prior to addition of cowpea mosaic virus (CPMV) or tobacco mosaic virus (TMV) particles. A) $(PEI\text{-}PAA)_{2.5}$ CPMV, B) $(PEI\text{-}PAA)_{2.5}$ TMV. In between each deposition step the crystal surface was rinsed with MilliQ water (*), and before and after deposition of the VNP sample the crystal was equilibrated and rinsed with the corresponding buffer (**). The frequency changes and dissipation shift measured for the third overtone of the resonance frequency are shown.

adsorption kinetics are inherent with differences in the viscoelastic properties of the assembly. Dissipative energy losses are high when TMV is deposited ($\Delta D \sim 29.9 \times 10^{-6}$) and low in the case of CPMV ($\Delta D \sim 3.3 \times 10^{-6}$). This indicates a more complex binding behaviour of TMV. Because of their anisotropic shapes it would be expected that the binding mode of the rods should be more complex than that of isotropic spheres; rods can bind in various conformations, such as flat or angled. The high changes in $\Delta D$ could imply conformational rearrangements of the particles until optimal binding and maximum coverage is achieved. The large changes in dissipation could also be attributable to a loosening of the layers due to interactions between the VNPs and polyelectrolytes.

### Multilayer LbL assembly of polyelectrolytes and a sphere-like VNP

Next, we investigated whether an alternating multilayer array of CPMV particles and polyelectrolytes could be assembled. The multilayer assembly studied was $(PEI\text{-}PAA)_{2.5}$ CPMV $(PEI\text{-}PAA)_n$ CPMV $(PEI\text{-}PAA)_2$, where $n$ was 2 or 3. The intermediate polyelectrolyte layers were chosen to be $n = 2$ or 3, because it was found that at least two intermediate bilayers of polyelectrolytes have to be added to allow binding of further CPMV particles (not shown). The monitored changes in $\Delta f$ and $\Delta D$ as the function of time monitored by QCMD, as well as the changes of absorbance with the number of layers as followed by UV/Vis spectroscopy, are summarized in Figure 2.

To determine the mass deposited, the Sauerbrey equation[14] was applied; further, for an estimation of layer thickness, data were modelled according to the Voigt model[15] by use of QTools software. Experimentally measured $\Delta m$ values and layer thickness ($h$), as well as the theoretical coverage expected for a closely packed CPMV monolayer, are given in Table 1.

The calculated $\Delta m$ values for each layer deposited are in good agreement; this indicates that similar amounts of VNPs bind in each deposition step. The experimentally ascertained values were higher than the theoretically expected mass coverage. Again, this is most probably due to water entrapped in cavities of the structure and hydrodynamically coupled water molecules. The particles were stably bound and desorption was not observed when the solution was replaced with either buffer or water; this is true for both VNP layers. The estimated layer thicknesses are in good agreement with the dimensions of the VNPs. CPMV has a spherically averaged diameter of about 30 nm. The slightly lower observed thickness may be due to the fact that the particles are, to some extent, embedded into the polyelectrolyte structures.

A striking feature in the QCMD plot is the increase in $\Delta f$, which corresponds to a decrease in $\Delta m$, after addition of the negatively charged PAA on top of the first VNP layer (Figure 2A). This phenomenon is observed after both VNP layers, but is more marked after the first VNP layer. This could imply displacement and solubilisation of the VNPs by the negatively charged polyelectrolyte chains. However, the dissipational changes were highest in this time regime. Relatively large positive $\Delta D$ shifts were recorded upon addition of PEI on top of the VNPs, and comparable negative $\Delta D$ values were recorded upon addition of PAA. This indicates that the multilayer underwent a transition from being viscous (highly hydrated) to being more rigid (fewer water molecules entrapped). The observed changes in $\Delta D$ and the inherent energy losses imply conformational changes; the increase in $\Delta f$ could therefore also be attributed to loss of water inherent with rearrangements within the array rather than solubilisation of biomolecules.

The QCMD data were overall in good agreement with the spectra recorded by UV/Vis spectroscopy (Figures 2B and C). Alternate deposition of the polyelectrolytes resulted in an increase in absorbance with each deposition step, with a peak of absorbance at about 240 nm (mainly attributable to PEI). Dep-

  

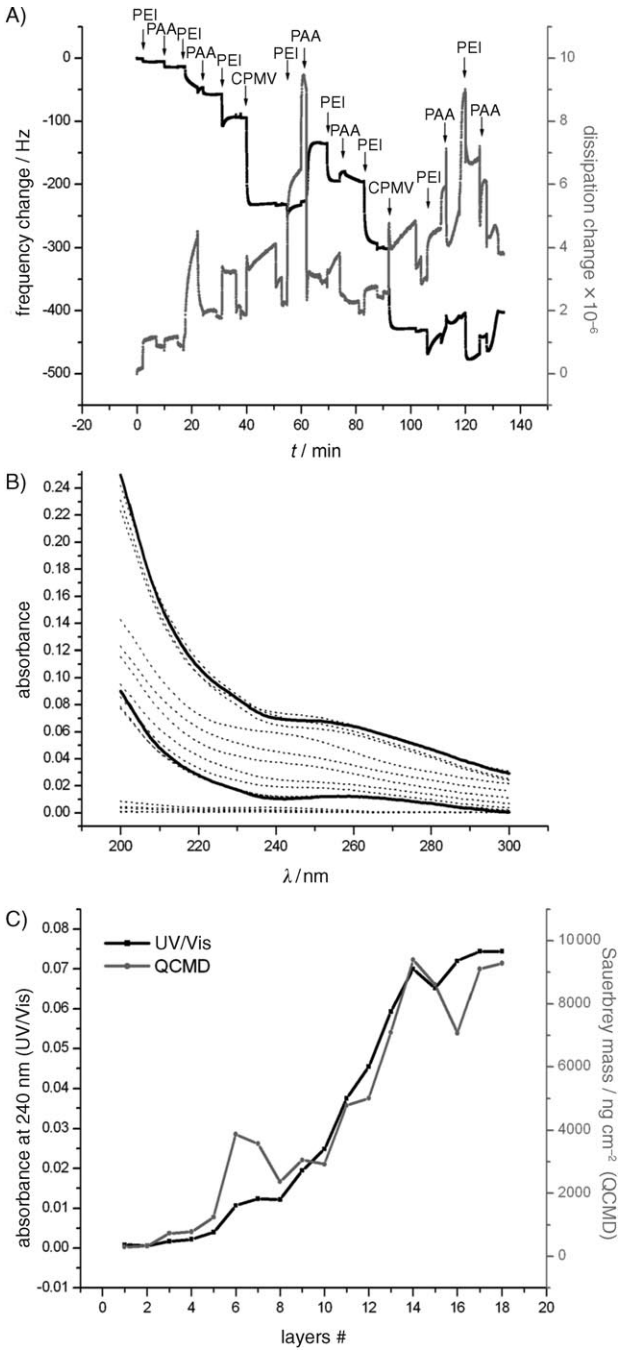


**Figure 2.** Build-up of polyelectrolyte multilayers with incorporated cowpea mosaic virus (CPMV) particles at pH 5.0, followed by quartz crystal microbalance frequency and dissipation (QCMD) and UV/Vis spectroscopy. The $(PEI\text{-}PAA)_{2.5}$ CPMV $(PEI\text{-}PAA)_n$ CPMV $(PEI\text{-}PAA)_2$ multilayer was studied, where $n$ was 2 or 3. A) Changes in frequency and dissipation monitored by QCMD, $n=2$. The frequency and dissipation changes measured for the third overtone of the resonance frequency are shown. B) Changes in absorption, monitored by UV/Vis studies; $n=3$. (Note: the values should be half for a single layer as the multilayer build-up takes place on both sides of the quartz slide.) Deposited CPMV is shown as solid lines, absorbance changes after addition of polyions as dotted lines. C) Comparison of QCMD ($n=3$) and UV/Vis spectroscopy data ($n=3$). The absorbance at absorption maximum (240 nm) versus the number of layers deposited is shown, together with the deposited mass, based on the Sauerbrey equation, versus the number of layers.

**Table 1.** Theoretical ($\Gamma$) and experimentally determined ($\Delta m$) coverage and thickness ($h$) of adsorbed polyelectrolytes and cowpea mosaic virus (CPMV) particles based on QCMD measurements.

| | $\Gamma$[a] [μg cm$^{-2}$] | $\Delta m$[b] [μg cm$^{-2}$] | $h$[c] [nm] |
|---|---|---|---|
| precursor $(PEI\text{-}PAA)_{2.5}$ film | N.A.[d] | N.A.[d] | 13.6 |
| 1st CPMV layer | 1.33 | 2.44 | 23.8 |
| intermediate $(PEI\text{-}PAA)_n$ film | N.A.[d] | N.A.[d] | $n=2$: 9.5<br>$n=3$: 27.4 |
| 2nd CPMV layer | 1.33 | 2.24 | 21.3 |

[a] Theoretical coverage for a closely packed CPMV monolayer. [b] Experimentally measured coverage based on the Sauerbrey equation. [c] Layer thickness based on the Voigt model. [d] N.A.: not applicable.

osition of CPMV particles resulted in an increase in absorbance, particularly at 260 nm and in the low-wavelength region. The absorbance maximum of VNPs was at 260 nm (due to the presence of RNA), and high absorbance in the lower-wavelength region (200–220 nm) was mainly derived from peptide bonds.

The apparent irregular changes in $\Delta f$ observed by QCMD after addition of the PAA on top of the bound VNPs were also reflected in the UV/Vis spectrum. It is noticeable that during the first steps of addition of polyelectrolytes on top of the immobilized VNPs, either no or only very little increase in absorbance was observed. VNPs are complex macromolecules, and although the overall charge on the particles is negative, the molecules are polyampholytes with regions of negative and positive charge produced by differently charged amino acids present on the particle surface. We propose that the low increase in absorbance in these initial steps is due to the low net charge density of the molecules, with only a few polyelectrolyte chains binding; once complete charge overcompensation is achieved then more regular build-up continues.

The topography of the $(PEI\text{-}PAA)_{2.5}$ CPMV $(PEI\text{-}PAA)_3$ thin films was imaged by SEM; in order to follow the sequential build-up a series of images were taken (Figure 3). The precursor film consisting of $(PEI\text{-}PAA)_{2.5}$ shows a smooth film with no distinct features. The deposited CPMV particles are adsorbed as a monolayer in a relatively dense conformation. The next series of images was taken after deposition of one and three bilayers of the polyions PEI and PAA, added on top of the immobilized CPMV particles. The SEM images show the adsorbing polyelectrolyte chains on top of the structure, covering the VNPs. The more polyelectrolytes were added, the smoother the film topology became and also gained in thickness. After three deposition steps, the VNPs were completely covered, except in the regions where the film was broken, which was probably an artefact from sample preparation. Imaging demonstrated that displacement of VNPs does not occur. This is particularly clear in those regions where scratches in the film reveal the VNP layer lying under the growing polyelectrolyte films. A second VNP layer was adsorbed, and imaging showed a topology similar to that observed for the first VNP layer.

Overall, the findings by QCMD, UV/Vis spectroscopy and SEM imaging are in good agreement and consistent with the multilayer build-up of polyions and the stable incorporation of

  

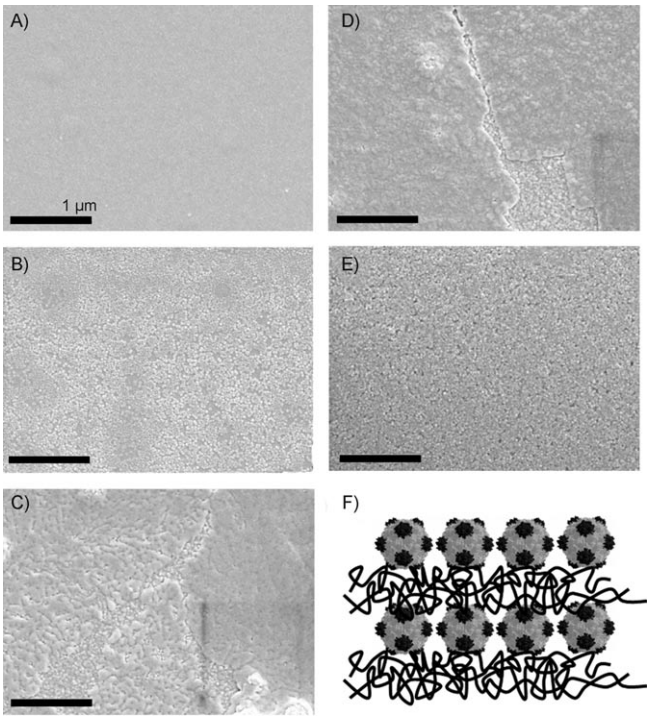


**Figure 3.** Scanning electron micrographs showing the sequential build-up of polyelectrolytes and cowpea mosaic virus (CPMV) particles. A) Precursor thin film consisting of 2.5 bilayers of the polyions linear poly(ethyleneimine) (PEI) and poly(acrylic acid) (PAA); B) $(PEI\text{-}PAA)_{2.5}$ CPMV; C) $(PEI\text{-}PAA)_{2.5}$ CPMV (PEI-PAA); D) $(PEI\text{-}PAA)_{2.5}$ CPMV $(PEI\text{-}PAA)_3$; E) $(PEI\text{-}PAA)_{2.5}$ CPMV $(PEI\text{-}PAA)_3$ CPMV; F) schematic representation of the architecture. All images were viewed at an acceleration voltage of 5 kV with a Zeiss Supra 55 VP FEG SEM; scale bar: 1 μm.

the sphere-like CPMV particles into the polyelectrolyte network.

### Role of particle shape in incorporation

To compare the alternating multilayer assembly mechanism of sphere-like CPMV with that of rod-shaped TMV particles with the aid of LbL techniques and polyelectrolytes, we investigated whether TMV particles could also be incorporated into polyelectrolyte multilayer assemblies under similar conditions. As with CPMV, TMV particles and the polyions PEI and PAA were used at pH 5.0. Initially, the build-up of the architecture followed the procedure outlined for CPMV with $(PEI\text{-}PAA)_{2.5}$ VNP $(PEI\text{-}PAA)_n$ VNP, with $n = 2$ or 3. However, we found that binding of the second TMV layer could not be achieved under these conditions (not shown).

Therefore, in a second series of experiments, the number of intermediate polyelectrolyte layers was increased until binding of further TMV particles could be observed. The following architectures were self-assembled: $(PEI\text{-}PAA)_{2.5}$ TMV $(PEI\text{-}PAA)_n$ TMV, whereby $n$ was 6 (not shown) and 12 (Figure 4). Build-up was followed by QCMD and UV/Vis spectroscopy.

Binding of TMV and subsequent polyelectrolytes is different. Overall, it was found that the first TMV layer was stably adsorbed on the polyion thin precursor film (no desorption upon rinsing with buffer and water), and additional polyions were

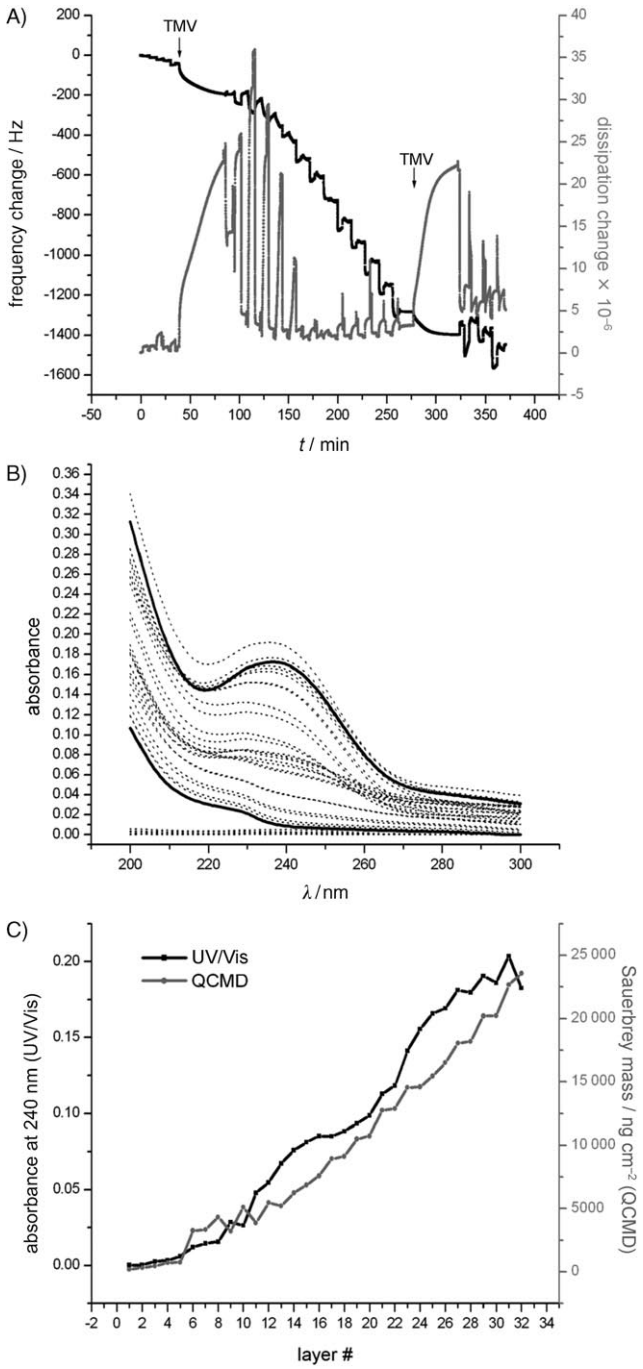


**Figure 4.** Build-up of polyelectrolyte multilayers with incorporated tobacco mosaic virus (TMV) particles at pH 5.0, followed by quartz crystal microbalance frequency and dissipation (QCMD) and UV/Vis spectroscopy. The following multilayer was studied: $(PEI\text{-}PAA)_{2.5}$ TMV $(PEI\text{-}PAA)_{12}$ TMV. A) Changes in frequency and dissipation measured by QCMD by use of the third overtone of the resonance frequency. B) Changes in absorption, monitored by UV/Vis spectroscopy. (Note: the values should be half for a single layer as the layer build-up takes place on both sides of the quartz slide.) Deposited TMV is shown as solid lines, absorbance changes after addition of polyions as dotted lines. C) Comparison of QCMD and UV/Vis spectroscopy data. The absorbance at absorption maximum (240 nm) versus the number of layers deposited, and the deposited mass, based on Sauerbrey, versus the number of layers are shown.

bound upon their addition on top of the immobilized VNP layer. Multiple intermediate bilayers of polyelectrolytes (at least

  

six) were needed before application of the second TMV layer in order to allow binding of the particles, although stable deposition of the second TMV layer was not achieved for any number of polyion bilayers studied. At low polyion bilayer numbers ($n<6$) no binding was observed; at higher number—for example, $n=12$—weak binding could be achieved (see discussion below). Binding of the first TMV layer was accompanied by large dissipation shifts; this indicates the transition from a relative rigid assembly of the precursor film into a hydrated and viscoelastic system. The adsorption of polyions on top of the first immobilized TMV layer was irregular in the initial steps; this is shown by the fluctuating changes in $\Delta f$ and $\Delta D$ recorded by QCMD and is indicated by a low increase in absorbance recorded by UV/Vis spectroscopy. The changes in $\Delta f$ increased when the polycation PEI was added and decreased when the polyanionic PAA was added. However, after four bilayers of (PEI-PAA) the system stabilized and a more continuous decrease in both $\Delta f$ and $\Delta D$ was observed for both types of polyions. The initial irregular changes in $\Delta f$ were accompanied by striking dissipative changes in $\Delta D$; this indicates structural changes (fluctuating transitions from a more rigid model to a viscoelastic system). Rearrangements of the VNPs or the assembly around the VNPs might also have an impact on the observed irregularities, and could explain why the deposition of a second TMV layer is difficult (if it can be achieved at all), especially when the number of intermediate polyelectrolyte bilayers is low.

The bindings of the first and second TMV layer were also different. The first TMV layer was stably bound onto the thin precursor film. This is indicated by the decrease in $\Delta f$ recorded by QCMD and also by the increase in absorbance measured by UV/Vis spectroscopy. However, the observations for the second deposited TMV layer were not as clear: QCMD data indicate that VNPs were only weakly bound and that most of the particles desorb upon rinsing with buffer and water. Also, the observed decrease in absorbance measured by UV/Vis spectroscopy implies that a second VNP layer was not deposited (Figure 4). The deposited $\Delta m$ for each VNP layer was calculated by using the Sauerbrey equation,[14] as well as the theoretical coverage ($\Gamma$) with the assumption of a closely packed TMV layer with the particles lying flat on the surface. Further, the average film thickness based on the Voigt model[15] was estimated; the values are listed in Table 2.

The calculated mass ($\Delta m$) deposited with the first TMV layer indicates the formation of a closely packed monolayer. The obtained value for $\Delta m$ was slightly higher than one would expect (see theoretical coverage); this could indicate that some particles are not flat on the surface or adsorb as bi- or multilayers in parts (SEM studies confirmed that in some regions particles indeed overlap with each other, Figure 5), or it could originate from water entrapped in cavities in the architecture. The latter situation is indicated by relatively large changes in $\Delta D$. The thickness calculated for the first TMV layer is in good agreement with the thickness of the particles, and indicates that the rods bind in a flat conformation, as confirmed by SEM imaging (Figure 5). The $\Delta m$ deposited for the second TMV layer is low and reaches only 34% of the $\Delta m$ deposited for the first TMV layer, thus showing that only a few particles are binding. This is also reflected in the estimated layer thicknesses and by UV/Vis spectroscopy, which did not indicate the adsorption of TMV particles when the second layer was added.

**Table 2.** Theoretical ($\Gamma$) and experimentally determined ($\Delta m$) coverage and thickness ($h$) of adsorbed polyelectrolytes and tobacco mosaic virus (TMV) particles based on QCMD measurements.

| | $\Gamma$[a] [μg cm$^{-2}$] | $\Delta m$[b] [μg cm$^{-2}$] | $h$[c] [nm] |
|---|---|---|---|
| precursor $(PEI\text{-}PAA)_{2.5}$ film | N.A.[a] | N.A.[a] | 8.7 |
| 1st TMV layer | 1.30 | 2.53 | 28.2 |
| intermediate $(PEI\text{-}PAA)_n$ film | N.A.[a] | N.A.[a] | 180.1 |
| 2nd TMV layer | 1.30 | 0.87 | 6.0 |

[a] Theoretical coverage for a closely packed CPMV monolayer. [b] Experimentally measured coverage based on the Sauerbrey equation. [c] Layer thickness based on the Voigt model. [d] N.A.: not applicable.

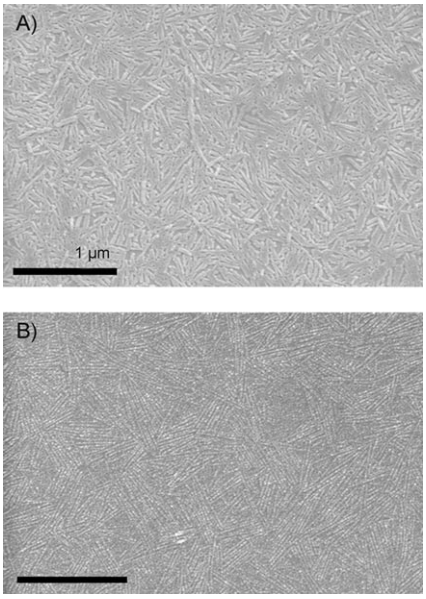


**Figure 5.** Scanning electron micrographs showing the sequential build-up of polyelectrolytes and tobacco mosaic virus (TMV) particles. A) $(PEI\text{-}PAA)_{2.5}$ TMV, and B) $(PEI\text{-}PAA)_{2.5}$ TMV $(PEI\text{-}PAA)_{12}$. All images were viewed at an acceleration voltage of 5 kV with a Zeiss Supra 55 VP FEG SEM; scale bar: 1 μm.

SEM imaging showed that TMV has a dramatically different architecture compared to that of CPMV (Figure 5). SEM studies showed that, as in the case of CPMV, a closely packed first TMV layer was immobilized onto the initial precursor film of polyelectrolytes; this is in good agreement with the findings from the QCMD measurements. Strikingly, however, in subsequent layers the deposited TMV particles—even after deposition of 12 interbilayers—were still visible on top of the architecture. The layer thickness of the intermediate 12 bilayers of (PEI-PAA) was estimated to be 180.1 nm (based on the Voigt model[15]). If stably bound onto the precursor film, the TMV particles should be completely covered by such a thick film of polyelectrolytes. The location of the particles on top of the

  

film suggests that the particles float through the multilayer film: they are excluded from the bulk of the multilayer and appear atop the architecture. These findings are consistent with the floating behaviour of M13.[6] Although sharing similarities, in being anisotropic rod-shaped particles, M13 and TMV have very different properties. The longer and thinner M13 particles have dimensions of ~800 nm in length and 6.5 nm in width. TMV, in contrast, has dimensions of 300 nm in length and 18 nm in width. In addition, the TMV rod is a stiff particle, whereas M13 is a flexible, filamentous rod. The net surface charges of M13 and TMV were negative in both experiments. The observation that the rod-shaped TMV particles—like M13, but unlike the spherical VNPs (CPMV, CCMV and CarMV)—float and are excluded from the architecture is very interesting. This behaviour could be common to rod-shaped particles. It would be interesting to incorporate mutations to further determine the relative contributions of charge and shape toward this behaviour.

The floating mechanism can be explained by interdiffusion of the polyelectrolytes.[6] It has been proposed that the PAA, which makes stronger electrostatic interactions with the PEI than the VNP, induces the separation process by competing with the VNP, and thus forces the VNP to the surface. Then, excluded volume and repulsive electrostatic interactions induce the spontaneous higher ordering on the surface. In addition to the floating, the particles appeared to be more ordered than those bound initially. The particles are aligned in patches (reminiscent of a smectic crystal). These observations are intriguing and may offer a starting point for the construction of highly organized VNP assemblies bound on polyelectrolyte films.

## Conclusions

In summary, we have demonstrated that negatively charged sphere-like and rod-shaped VNPs can be immobilized on polyelectrolyte assemblies. The assembly mechanisms of multilayered arrays of alternating VNPs and polyelectrolytes were markedly influenced by the shape of the VNP. Sphere-like CPMV particles showed rapid adsorption kinetics. Further, sphere-like VNPs can be incorporated into the architecture; that is, an alternate structure of polyelectrolytes and VNPs can be self-assembled. In stark contrast, rod-shaped particles showed slow adsorption kinetics with inherent dissipative energy losses; this indicates structural rearrangements in the array. Most interestingly, TMV particles were found to be floating atop the architecture when further polyions were deposited on top of immobilized VNPs, and spontaneous ordering on the surface was observed.

In this paper we have used three independent physical methods—QCMD, UV/Vis spectroscopy and SEM—in order to follow LbL assembly. Further characterization methods including atomic force microscopy, small angle X-ray scattering, cross-sectional transmission electron microscopy, Fourier-transform infrared spectroscopy and ellipsometry should in the future help in providing further insights into the properties of the assembled arrays. In addition, systematic studies at varying pH values, as well as the use of VNP mutants with different surface properties, would be expected to give further clues about the mechanisms involved. Last, but not least, a study that uses spheres and rods formed by the same viral coat protein would be helpful for explaining whether the "floating" mechanism is based on the shape of the virion. Even in this case, however, one would have to keep in mind that although formed by the same coat protein, subtle differences in surface charge between sphere and rod might still occur due to differences in the conformations and orientations of the proteins.

The observed phenomenon that rod-shaped TMV particles floated on top of the architecture whereas sphere-like CPMV particles were incorporated into the assembly is interesting and in good agreement with previous studies with CCMV, CarMV and M13. This paper, along with previous data, indicates that the floating behaviour of rod-shaped particles might be a common feature of such particles. A potential molecular explanation is that the floating is initiated by interdiffusion of the polyelectrolytes. The polyelectrolytes rearrange and thus induce a separation process that forces TMV particles to float on top of the structure. The question still remains as to why TMV particles float whereas CPMV particles do not. The most obvious difference between the two VNPs is their size and shape. However, although their pIs are similar, subtle differences in surface charge, especially in the local charge distribution on the capsid surface, will also have an impact on the molecular mechanisms involved in the binding mode.

In physics, buoyancy, the upward force of an object in a fluid, is dependent on the density of the fluid and on the density and the surface area of the object itself. The densities of CPMV and TMV particles are comparable (~400 $g\,mol^{-1}\,nm^{-3}$), in stark contrast to the surface area—the TMV rod has a surface area of 22200 $nm^2$ while that of the CPMV sphere is only 2800 $nm^2$. This large difference of almost an order of magnitude would be expected to have a significant impact on the physical properties of the particles both in solution and when embedded in flexible and tunable polyelectrolyte multilayers. Since their structural properties are strikingly different, we hypothesize that the different behaviour of TMV and CPMV particles in the assembly can be attributed to their structural properties rather than to their different surface chemistries. This hypothesis is supported by the floating behaviour of M13, which has a surface area comparable to that of TMV, at 18000 $nm^2$.

VNPs are popular tools for materials science, and we[10,11,17] and others[18] have previously demonstrated the feasibility of VNPs as a platform for chemical modification with a broad range of molecules, with potential applications that range from biomedicine to electronics. The incorporation of functionalized VNPs and polyelectrolytes would be expected to offer new exciting routes for the design and construction of nanostructured tuneable films. Therefore, it is important to understand fundamental principles of VNP self-assembly mechanisms in thin films. In the field of nanotechnology it is commonly known that materials' properties are strongly dependent on the size of matter. Now, our data suggest that shape matters, too.

  

## Experimental Section

**Polyelectrolytes**: Poly(ethyleneimine) (PEI, linear, $M_W$ 25.0 kDa; Polysciences) and poly(acrylic acid) (PAA, $M_W$ 90.0 kDa, Acros Scientific) were used as aqueous solutions (2 mM). NaCl (30 mM) was added, and the pH was adjusted to pH 5.0.

**Virus growth and purification**: The propagation and purification of CPMV virions was performed by standard procedures.[19] TMV particles were provided by Prof. Rainer Fischer (RWTH–Aachen University, Germany). Purified CPMV and TMV particles were stored at 4 °C in sodium phosphate buffer (pH 7.0, 10 mM). The concentration of purified virions was determined by Bradford assay or photometrically. In all experiments the particles were used at a concentration of 1 mg mL$^{-1}$ in sodium phosphate buffer (pH 5.0, 10 mM).

**QCMD studies**: The build-up of the hydrated multilayer structures was characterized with a quartz crystal microbalance with dissipation monitoring (QCMD, model D300, Q-Sense AB, Västra Frölunda, Sweden) with a QAFC 302 axial flow measurement chamber. An AT-cut piezoelectric quartz crystal (cut at 35° to the *y*-axis) sandwiched between two gold electrodes was used as sensing element. For all measurements silica-coated QCMD chips were used. The crystal is excited to its fundamental resonant frequency at ~5 MHz. The QCMD chips were first immersed and washed several times with MilliQ water. After stabilization of the fundamental resonance frequency of the quartz crystal the thin film was prepared by alternate addition of PEI and either PAA or the VNP solution. In between each deposition step the crystal was washed with MilliQ water in order to remove any loosely adsorbed polymers or VNPs. Before and after introduction of VNPs into the system the film was exposed to the sodium phosphate buffer (pH 5.0, 10 mM). Data were analysed both approximately by use of the Sauerbrey equation[14] and more precisely by use of a Voigt continuum model[15] fitted with the QTools program (Q-Sense AB, Västra Frölunda, Sweden).

**UV/Vis spectroscopy**: For UV/Vis spectroscopy the polyelectrolyte films were constructed on quartz slides (light path 1 mm). The slides were immersed in a $H_2O_2$/concentrated $H_2SO_4$ mixture 30:70 (30% *w/v*) for 1 h at 80 °C. This treatment—also known as piranha etch treatment—leads to the exposure of free silanol groups on the substrate surface, which was subsequently deprotonated at pH > 3, and resulted in an overall negatively charged surface.[20] ***CAUTION!*** *Piranha is highly corrosive and reacts violently with organic materials; solutions should be handled with extreme care and only small volumes should be prepared at any one time.* After this treatment the slides were rinsed several times with MilliQ water in order to remove the piranha etch solution. The polyelectrolyte multilayers were constructed as follows: the prepared slides were immersed in an aqueous PEI solution (2 mM, 30 mM NaCl, pH 5.0) for 5 min at room temperature, and were then rinsed with MilliQ water for 2 min. The slides were then immersed in an aqueous PAA solution ($M_W$ 90 000, 2 mM, 30 mM NaCl pH 5.0) for 5 min at room temperature, and were again rinsed with MilliQ water. This resulted in the formation of a bilayer. These steps were then repeated until the desired number of layers was achieved. Absorption measurements were obtained for each layer between wavelengths of 200 and 300 nm on a Perkin–Elmer Lambda 25 spectrophotometer. UV/Vis measurements were taken after each step in the layer build-up, after the slides were rinsed in MilliQ water and dried with a stream of nitrogen.

**Scanning electron microscopy (SEM)**: Either the same slides from the UV/Vis measurements were imaged, or thin films were prepared by the procedure described above. Films were constructed on quartz slides or on glass surfaces after piranha etch treatment. These samples were then mounted on the surface of an aluminium pin stub with use of double-sided adhesive carbon discs (Agar Scientific, Ltd., Stansted, UK). The stubs were then sputter-coated with gold (approximately 15 nm) in a high-resolution sputter coater (Agar Scientific, Ltd.) and transferred to a Zeiss Supra 55 VP FEG scanning electron microscope (Zeiss, SMT, Germany). The samples were viewed at 5 kV and digital TIFF files were stored.

## *Acknowledgements*

*Prof. Marianne Manchester (The Scripps Research Institute, La Jolla, USA) is thanked for helpful discussions and editing the manuscript. Prof. Rainer Fischer (RWTH–Aachen University, Germany) is thanked for providing the TMV. Sue Bunnewell is thanked for technical assistance with the EM, J. Elaine Barclay (John Innes Centre, UK) is thanked for help with CPMV preparations. This work was funded by the BBSRC (K.C.F., G.P.L., D.J.E.), the Core Strategic Grant of the BBSRC (T.R.N., R.P.), and the EU grant MEST-CT-2004–504 273 (N.F.S.).*

**Keywords:** immobilization · nanostructures · polyions · self-assembly · viral nanoparticles

[1] G. Decher, *Science* **1997**, *277*, 1232–1237.
[2] F. Caruso, K. Niikura, D. N. Furlong, Y. Okahata, *Langmuir* **1997**, *13*, 3427–3433; Y. Lvov, K. Ariga, I. Ichinose, T. Kunitake, *J. Am. Chem. Soc.* **1995**, *117*, 6117–6123; M. Onda, Y. Lvov, K. Ariga, T. Kunitake, *Biotechnol. Bioeng.* **1996**, *51*, 163–167.
[3] Y. Lvov, G. Decher, G. Sukhorukov, *Macromolecules* **1993**, *26*, 5396–5399.
[4] S. Joly, R. Kane, L. Radzilowski, T. Wang, A. Wu, R. E. Cohen, E. L. Thomas, M. F. Rubner, *Langmuir* **2000**, *16*, 1354–1359; T. Cassagneau, J. H. Fendler, T. E. Mallouk, *Langmuir* **2000**, *16*, 241–246.
[5] M. Ginzburg, J. Galloro, F. Jäkle, K. N. Power-Billard, S. Yang, I. Sokolov, C. N. C. Lam, A. W. Neumann, I. Manners, G. A. Ozin, *Langmuir* **2000**, *16*, 9609–9614; J. B. Schlenoff, D. Laurent, H. Ly, J. Stepp, *Adv. Mater.* **1998**, *10*, 347–249.
[6] P. J. Yoo, K. T. Nam, J. F. Qi, S. K. Lee, J. Park, A. M. Belcher, P. T. Hammond, *Nat. Mater.* **2006**, *5*, 234–240.
[7] Y. Lvov, H. Haas, G. Decher, H. Möhwald, *Langmuir* **1994**, *10*, 4232–4236.
[8] P. A. Suci, M. T. Klem, F. T. Arce, T. Douglas, M. Young, *Langmuir* **2006**, *22*, 8891–8896.
[9] N. F. Steinmetz, D. J. Evans, *Org. Biomol. Chem.* **2007**, *5*, 2891–2902; T. Douglas, M. Young, *Science* **2006**, *312*, 873–875; M. Manchester, P. Singh, *Adv. Drug Delivery Rev.* **2006**, *58*, 1505–1522.
[10] N. F. Steinmetz, G. Calder, G. P. Lomonossoff, D. J. Evans, *Langmuir* **2006**, *22*, 10032–10037.
[11] N. F. Steinmetz, E. Bock, R. P. Richter, J. P. Spatz, G. P. Lomonossoff, D. J. Evans, *Biomacromolecules* **2008**, *9*, 456–462.
[12] http://www.dpvweb.net
[13] R. G. Smits, G. J. M. Koper, M. Mandel, *J. Phys. Chem.* **1993**, *97*, 5745–5751.
[14] G. Sauerbrey, *Z. Phys.* **1959**, *155*, 206–222.
[15] M. V. Voinova, M. Rodahl, M. Johnson, B. Kasemo, *Phys. Scr.* **1999**, *59*, 391–396.
[16] F. Höök, M. Rodahl, P. Brzezinski, B. Kasemo, *Langmuir* **1998**, *14*, 729–734; F. Höök, J. Vörös, M. Rodahl, R. Kurrat, P. Böni, J. J. Ramsden, M. Textor, N. D. Spencer, P. Tengvall, J. Gold, B. Kasemo, *Colloids Surf. B* **2002**, *24*, 155–170.
[17] N. F. Steinmetz, D. J. Evans, G. P. Lomonossoff, *ChemBioChem* **2007**, *8*, 1131–1136; N. F. Steinmetz, G. P. Lomonossoff, D. J. Evans, *Small* **2006**, *2*, 530–533; N. F. Steinmetz, G. P. Lomonossoff, D. J. Evans, *Langmuir* **2006**, *22*, 3488–3490.
[18] D. M. Kuncicky, R. R. Naik, O. D. Velev, *Small* **2006**, *2*, 1462–1466; J. D. Lewis, G. Destito, A. Zijlstra, M. J. Gonzalez, J. P. Quigley, M. Manchester,

  

H. Stuhlmann, *Nat. Med.* **2006**, *12*, 354–360; C. Mao, D. J. Solis, B. D. Reiss, S. T. Kottmann, R. Y. Sweeney, A. Hayhurst, G. Georgiou, B. Iverson, A. M. Belcher, *Science* **2004**, *303*, 213–217; K. T. Nam, D. W. Kim, P. J. Yoo, C. Y. Chiang, N. Meethong, P. T. Hammond, Y. M. Chiang, A. M. Belcher, *Science* **2006**, *312*, 885–888; D. E. Prasuhn, Jr., R. M. Yeh, A. Obenaus, M. Manchester, M. G. Finn, *Chem. Commun.* **2007**, 1269–1271; K. S. Raja, Q. Wang, M. G. Finn, *ChemBioChem* **2003**, *4*, 1348–1351; C. M. Soto, A. S. Blum, G. J. Vora, N. Lebedev, C. E. Meador, A. P. Won, A. Chatterji, J. E. Johnson, B. R. Ratna, *J. Am. Chem. Soc.* **2006**, *128*, 5184–5189; A. Chatterji, W. Ochoa, L. Shamieh, S. P. Salakian, S. M. Wong, G. Clinton, P. Ghosh, T. Lin, J. E. Johnson, *Bioconjugate Chem.* **2004**, *15*, 807–813; A. Chatterji, W. F. Ochoa, M. Paine, B. R. Ratna, J. E. Johnson, T. Lin, *Chem. Biol.* **2004**, *11*, 855–863; Q. Wang, T. R. Chan, R. Hilgraf, V. V. Fokin, K. B. Sharpless, M. G. Finn, *J. Am. Chem. Soc.* **2003**, *125*, 3192–3193; Q. Wang, T. Lin, L. Tang, J. E. Johnson, M. G. Finn, *Angew. Chem.* **2002**, *114*, 477–480; *Angew. Chem. Int. Ed.* **2002**, *41*, 459–462; M. Fischlechner, U. Reibetanz, M. Zaulig, D. Enderlein, J. Romanova, S. Leporatti, S. Moya, E. Donath, *Nano Lett.* **2007**, *7*, 3540–3546.

[19] J. Wellink, *Methods Mol. Biol.* **1998**, *81*, 205–209.

[20] M. S. Johal, B. H. Ozer, J. L. Casson, A. St. John, J. M. Robinson, H.-L. Wang, *Langmuir* **2004**, *20*, 2792–2796.

Received: January 31, 2008
Published online on June 6, 2008

  